

Electron dynamics in gold and gold–silver alloy nanoparticles: The influence of a nonequilibrium electron distribution and the size dependence of the electron–phonon relaxation

S. Link and C. Burda

Laser Dynamics Laboratory, School of Chemistry and Biochemistry, Georgia Institute of Technology, Atlanta, Georgia 30332-0400

Z. L. Wang

School of Materials Science and Engineering, Georgia Institute of Technology, Atlanta, Georgia 30332-0400

M. A. El-Sayed^{a)}

Laser Dynamics Laboratory, School of Chemistry and Biochemistry, Georgia Institute of Technology, Atlanta, Georgia 30332-0400

(Received 8 February 1999; accepted 19 April 1999)

Electron dynamics in gold nanoparticles with an average diameter between 9 and 48 nm have been studied by femtosecond transient absorption spectroscopy. Following the plasmon bleach recovery after low power excitation indicates that a non-Fermi electron distribution thermalizes by electron–electron relaxation on a time scale of 500 fs to a Fermi distribution. This effect is only observed at low excitation power and when the electron distribution is perturbed by mixing with the intraband transitions within the conduction band (i.e., when the excitation wavelength is 630 or 800 nm). However, exciting the interband transitions at 400 nm does not allow following the early electron thermalization process. Electron thermalization with the lattice of the nanoparticle by electron–phonon interactions occurs within 1.7 ps under these conditions, independent of the excitation wavelength. In agreement with the experiments, simulations of the optical response arising from thermalized and nonthermalized electron distributions show that a non-Fermi electron distribution leads to a less intense bleach of the plasmon absorption. Furthermore, the difference between the response from the two electron distributions is greater for small temperature changes of the electron gas (low excitation powers). No size dependence of the electron thermalization dynamics is observed for gold nanoparticles with diameters between 9 and 48 nm. High-resolution transmission electron microscopy (HRTEM) reveals that these gold nanoparticles possess defect structures. The effect of this on the electron–phonon relaxation processes is discussed. 18 nm gold–silver alloy nanoparticles with a gold mole fraction of 0.8 are compared to 15 nm gold nanoparticles. While mixing silver leads to a blue-shift of the plasmon absorption in the ground-state absorption spectrum, no difference is observed in the femtosecond dynamics of the system. © 1999 American Institute of Physics. [S0021-9606(99)71427-3]

INTRODUCTION

Electron dynamics in small metal and semiconductor nanoparticles probed by femtosecond spectroscopy techniques has recently drawn much attention,^{1–15} aiming at understanding size effects in small particles as well as searching for novel devices for optoelectronic and microelectronic applications.^{16,17} Several authors have investigated metallic and in particular gold nanoparticles in solution as well as embedded in a solid matrix.^{2–16} After laser excitation, gold nanoparticles show a bleach of the plasmon band due to heating of the electron gas. Ahmadi *et al.*^{2,3} measured decay times of 2.5 and >50 ps for the electron–phonon and phonon–phonon interactions, respectively, in 30 nm gold particles in water when exciting at 380 and 600 nm and

probing at the plasmon resonance. They also found that the observed lifetimes are power dependent and increase with increasing laser power as a larger amount of heat has to be transferred to the surrounding medium. Perner *et al.*^{4,5} reported relaxation times of 4 and 200 ps for 30 nm gold particles embedded in a sol-gel matrix after excitation at 400 nm. Inouye *et al.*¹⁴ measured gold nanoparticles with a diameter of 7.6 nm in a SiO₂ glass matrix and found decay times of 2.8 and 120 ps. Smith *et al.*^{11–13} on the other hand observed longer relaxation times of 7 and 400 ps for 15 nm gold particles in water when probed at 790 nm after excitation at 390 nm. They also reported a reduction of the decay time for electron–phonon interactions from 7 to 3.5 ps when the solvent was cyclohexane.

Although these results seem to compare reasonably well with each other, the minor differences in the reported decay times might be due to differences in sizes and size distributions, the different surrounding media, differences in the

^{a)} Author to whom correspondence should be addressed. Electronic mail: mostafa.el-sayed@chemistry.gatech.edu

technique used (i.e., transient absorption vs bleach recovery), and also due to differences in the power of the excitation laser. The lifetime of the transient absorption signal increases with increasing laser power^{3,7} and a detailed power series was carried out by Hodak *et al.*^{7,8} on 11 nm gold particles, which shows that the electron–phonon relaxation time depends linearly on the laser power for the low excitation limit. Their experiments yielded a limiting decay time of 0.7 ± 0.1 ps for the electron–phonon interactions.

Feldstein *et al.*¹⁸ have studied the electron relaxation dynamics in a series of thin films prepared by wet chemistry techniques from 12 nm gold nanoparticles. The measured lifetimes for the electron–phonon interactions range from 1 to 3 ps decreasing with greater aggregation. This indicates that the concentration or volume fraction (domain size) of the metal nanoparticles is also an important factor when comparing measured lifetimes.

Lifetimes of 1–4 ps for the electron–phonon interactions in gold nanoparticles and the observed power dependence are in very good agreement with measurements on bulk gold films.^{19–38} However, by using femtosecond transient transmissivity and reflectivity as well as time-resolved photoemission spectroscopy on thin gold films, several authors showed that the initially created non-Fermi electron distribution internally thermalizes to a Fermi distribution by electron–electron scattering on a finite time scale (longer than the excitation pulse) and can be resolved using these femtosecond techniques.^{19,23,24,34,35} Sun *et al.*^{23,24} found a thermalization time of 500 fs for 20 nm films. Fann *et al.*^{34,35} reported a value of 700 fs for 30 nm gold films, which can be as long as 1 ps when lowering the excitation power (note that this behavior is opposite to the one for the electron–phonon interactions). The internal electron thermalization time is, therefore, of the same magnitude as the external thermalization of the hot electrons via electron–phonon interactions.

This fact of a finite electron thermalization time has so far not been addressed for gold nanoparticles in colloidal solution. Here, we report for the first time the detection and modeling of a non-Fermi electron distribution in gold nanoparticles. The size dependence of the electron dynamics is further evaluated in the same medium and in a size range comparable to the mean free path of the conduction electrons where electron-surface scattering is expected to be the dominant relaxation process. In addition we discuss the influence of alloy formation between gold and silver on the hot electron dynamics.

EXPERIMENT

The synthesis of the gold nanoparticles with mean diameters between 9 and 48 nm and their characterization by transmission electron microscopy (TEM) and optical absorption spectroscopy have been described elsewhere.³⁹ Briefly, the synthesis of the gold nanoparticles with an average diameter of about 20 nm involved the reduction of chlorauric acid HAuCl_4 in a boiling aqueous solution by adding sodium citrate.⁴⁰ In order to produce smaller nanoparticles the order of addition was reversed.⁴¹ Larger particles were obtained by reduction of HAuCl_4 with hydroxylamine hydrochloride in the presence of the already synthesized 20 nm particles.^{42,43}

Gold–silver alloy nanoparticles were prepared by the co-reduction of chlorauric acid and silver nitrate AgNO_3 with sodium citrate in aqueous solution. Their characterization and optical properties have also been described elsewhere.⁴⁴

In order to increase the optical density (OD) of the different samples (final OD of about 0.8 in a 2 mm cell at the plasmon absorption maximum) the solutions were concentrated after the nanoparticles had been coated with a polymer (polyethylene glycol, molecular weight 10 000). The coating was simply achieved by stirring a mixture of the nanoparticles and the polymer for 1 h.⁴⁵ This is necessary because the stabilization by the excess citrate molecules is not sufficient and concentrating the samples would under normal circumstances lead to aggregation before the desired optical density is reached. Aggregation is also favored at low pH values and high electrolyte (salt) concentrations.⁴¹ As the synthesis of the larger particles results in HCl as a byproduct, these solutions were first neutralized and then the ions were removed by chromatography with deionized water and dialysis molecularporous membrane tubing (Spectra/Por, VWR Scientific, molecular weight cutoff 12 000–14 000).

The femtosecond transient spectroscopy experiments were carried out as follows: An amplified Ti-Sapphire laser system (Clark MXR CPA 1000) was pumped by an argon ion laser (Coherent Innova 100). This produced laser pulses of 100 fs duration (HWFEM) and an energy of 1 mJ at 790 nm. The repetition rate was 1 kHz. A small part (4%) of the fundamental was used to generate a white light continuum in a 1 mm sapphire plate. The remaining laser light was split into two equal parts in order to pump two identical OPAs (Quantronix TOPAS). Each produced signal and idler waves with a total energy of 150 μJ . Tunable excitation wavelengths in the visible range were then produced by second-harmonic generation (SHG) and sum-frequency generation (SFG) of the signal wave. The excitation beam was modulated by an optical chopper (HMS 221) with a frequency of 500 Hz. The second OPA was used to generate tunable probe wavelengths outside the continuum range. The probe light was split into a signal and a reference beam. After passing the monochromator (Acton Research) both beams were detected by two photodiodes (Thorlab). The kinetic traces were obtained using a sample-and-hold unit and a lock-in-amplifier (Stanford Research Systems). The typical measured optical density (OD) changes were in the range of 5–50 mOD. For spectral measurements a CCD camera (Princeton Instruments) attached to a spectrograph (Acton Research) was used. The group velocity dispersion of the white light continuum was compensated.

The size of the particles is analyzed by TEM using a Hitachi HF-2000 field emission TEM operating at 200 kV. From the TEM images the size distributions of the different samples are determined by counting at least 300 particles. The high resolution TEM (HRTEM) studies are carried out with a JEOL 4000 EX HRTEM operating at 400 kV. The UV-Vis absorption spectra are recorded on a Beckman DU 650 spectrophotometer in a 1 cm glass cuvette.

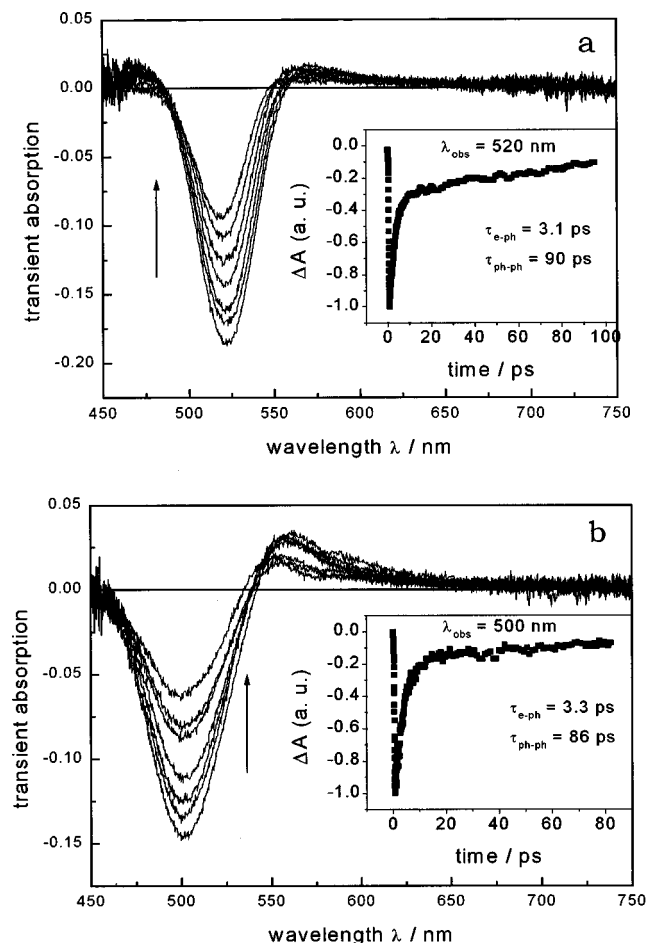


FIG. 1. (a) Transient absorption spectra of 15 nm gold nanoparticles after excitation with 400 nm laser pulses of 100 fs duration at different delay times. The inset shows the decay of the plasmon band bleach followed at the bleach maximum at 520 nm. A biexponential fit gave decay times of 3.1 and 90 ps for the electron-phonon (e-ph) and phonon-phonon (ph-ph) interactions. (b) Transient absorption spectra of 18 nm gold-silver alloy nanoparticles ($x_{\text{Au}}=0.8$) after excitation with 400 nm laser pulses of 100 fs duration at different delay times. The inset shows the decay of the plasmon band bleach followed at the bleach maximum at 500 nm. A biexponential fit gave decay times of 3.3 and 86 ps for the electron-phonon (e-ph) and phonon-phonon (ph-ph) interactions.

RESULTS AND DISCUSSION

Alloy nanoparticles

As described in reference 44 gold and silver form alloy nanoparticles of similar size and structure as pure gold nanoparticles prepared in the same way. The plasmon absorption of these alloy particles, however, depends linearly on the composition of the alloy particles when expressed in terms of the gold mole fraction x_{Au} . In Fig. 1 the electron dynamics in gold and gold-silver alloy nanoparticles are compared. A higher temperature of the electron gas of a metal nanoparticle leads to a broadening of the surface plasmon resonance and a decrease in the maximum intensity. This then results in a bleach at the position of the plasmon absorption maximum and two positive absorptions to the blue and to the red of the plasmon band in the transient absorption spectrum as shown for 15 nm gold nanoparticles in Fig. 1(a). The excitation wavelength is 400 nm. The inset illustrates the decay of the

bleach signal at 520 nm. Two components of the hot electron relaxation with decay times of 3.1 and 90 ps are clearly visible and reflect the electron-phonon and phonon-phonon interactions, respectively, which lead to the electron cooling of the nanoparticle system and the decay of the transient bleach. In Fig. 1(b) the corresponding results for 18 nm gold-silver alloy nanoparticles with a composition of $x_{\text{Au}}=0.8$ are shown. The relaxation of the hot electron gas in these alloy nanoparticles is found to be very similar to the pure gold particles with decay times of 3.3 and 86 ps when monitored at the bleach maximum [500 nm, see inset of Fig. 1(b)]. The experimental conditions such as optical density and laser fluence are identical for the two samples except for the small difference in size, which should not change our results considering the results on the size dependence of the electron dynamics (see below). It can therefore be concluded that admixture of silver only changes the spectral position of the plasmon band bleach but has no observable effect on the electron cooling rate in gold-silver alloy nanoparticles. This fact enables one to tune the optical properties of the gold-silver system in a controlled manner. It might also be of interest for ultrafast applications.

Internal electron thermalization

The aspect of a finite internal thermalization time of an initially non-Fermi electron distribution has not been addressed in detail so far in gold nanoparticles. However, by varying the excitation wavelength the effect of different non-Fermi electron distributions on the internal electron thermalization can be followed when low excitation powers are used. According to Fermi liquid theory⁴⁶ the electron-electron scattering rate is proportional to the square of the energy difference between the excited electron and the Fermi energy. The scattering rate is therefore faster for highly excited electrons as more unoccupied states are available (greater available k -space) and slows down considerably for electrons close to the Fermi level. The electron-electron scattering time is usually on the order of 10 fs.⁴⁶⁻⁴⁸ The thermalization time of the non-Fermi electron distribution includes then all scattering events of the excited electrons until a Fermi distribution is reached.

In Fig. 2 the decay of the bleach at 530 nm in 22 nm gold nanoparticles is compared when the excitation wavelength is (a) 400 nm, (b) 630 nm, and (c) 800 nm. It was attempted to fit the experimental data with a monoexponential decay for the electron-phonon relaxation time after deconvolution with a 100 fs excitation pulse [solid line in Fig. 2(a) and dashed lines in Figs. 2(b) and 2(c), lifetimes of 1.7, 1.8, and 1.8 ps for Figs. 2(a)-2(c), respectively]. While good agreement for 400 nm excitation is achieved, a monoexponential decay cannot reproduce the other two kinetic traces. Especially the curve in Fig. 2(c), displaying the optical response after 800 nm excitation, shows a pronounced deviation in the first 2 ps. It actually decays slower in the first few picoseconds suggesting a finite rise time of the maximum transient transmission signal. This behavior is further emphasized by the residuals for the two fits to Fig. 2(c) plotted in Fig. 2(d).

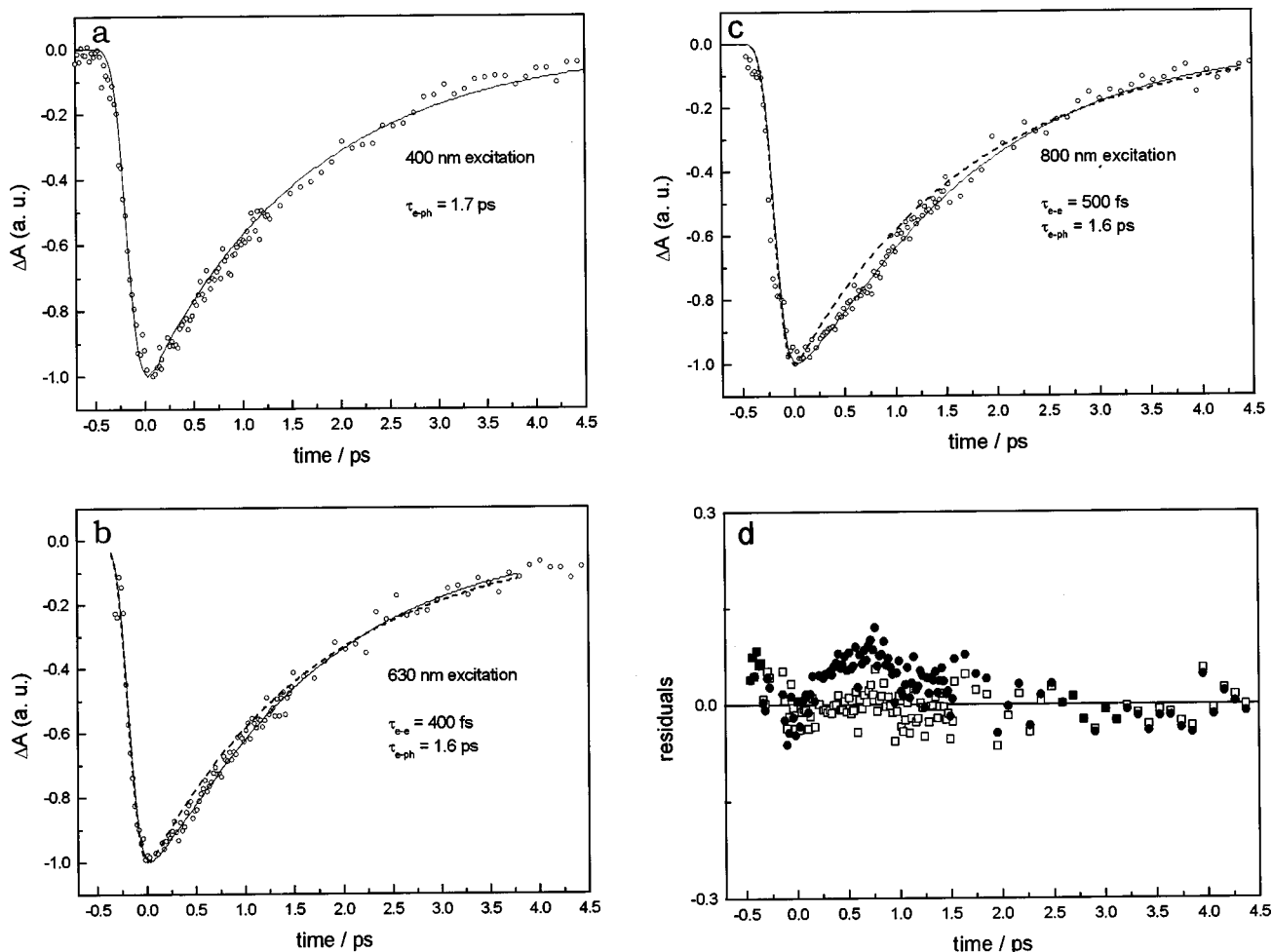


FIG. 2. Plasmon bleach recovery of 22 nm gold particles monitored at 530 nm after exciting at 400 nm (a), 630 nm (b), and 800 nm (c). The solid line in part (a) is a monoexponential fit with a decay time of 1.7 ps. The solid lines in parts (b) and (c), however, represent fits with Eq. (1) giving electron thermalization times τ_{e-e} of 400 fs (b) and 500 fs (c) and an electron-phonon relaxation time τ_{e-ph} of 1.6 ps for both experimental curves. The dotted lines in (b) and (c) are monoexponential fits with a lifetime of 1.8 ps. The monoexponential fits clearly cannot reproduce the experimental data for the early part of the transient signal. This is also illustrated in part *d* where the residuals (difference between experimental and fit value) for the two fits in (c) are plotted [closed circles: Monoexponential fit; open squares: Fit with Eq. (1)].

The observed behavior can, however, be modeled by a rate equation derived by Sun *et al.*²³ Their model consists of a modification to the two-temperature model (TTM⁴⁹) which describes the system by a set of coupled differential equations. They assume for the nonthermal electron distribution that the contribution of the nonthermal electrons is proportional to their integrated energy density. This approach, which describes the nonthermal electron distribution by a unique energy-associated time constant, is equivalent to using a time-averaged electron distribution function. With this approximation, the response function at the probe photon energy $h\nu$ can be expressed as

$$\frac{\Delta T}{T}(h \cdot \nu) = \left[\frac{\Delta T}{T}(h \cdot \nu) \right]_{NT} \cdot \exp\left(-\frac{t}{\tau'_{th}}\right) + \left[\frac{\Delta T}{T}(h \cdot \nu) \right]_{Th} \cdot \exp\left(-\frac{t}{\tau_p}\right) \cdot \left\{ 1 - \exp\left(-\frac{t}{\tau_{th}}\right) \right\}, \quad (1)$$

with $1/\tau'_{th} = 1/\tau_{th} + 1/\tau_p$. τ_{th} is defined as the thermalization time of the electrons while the temperature of the thermalized distribution decays due to electron-phonon interactions

with time constant $1/\tau_p$. The rise time of the thermalized distribution τ_{th} being longer than the decay time of the nonthermal population τ'_{th} reflects the fact that the nonthermalized electron distribution interacts with the phonon bath during the thermalization process. The subscripts NT and Th of the amplitudes in Eq. (1) stand for nonthermal and thermalized, respectively.

Although this approach neglects the energy dependence of the electron relaxation, it permits a simple, qualitative description of the electron dynamics. Sun *et al.*²³ have found very good agreement between their measured data with those predicted by this rate equation model. This fitting routine was therefore used to analyze the recorded data and gave indeed a much better fit to the measured decay in Figs. 2(b) and 2(c) (solid lines, note that small changes in the differential transmission $\Delta T/T$ are equal to changes in the absorbance ΔA). From the obtained fitting parameters a thermalization time τ_{th} of 400 and 500 fs and an electron-phonon relaxation time τ_p of 1.6 ps are calculated for 630 nm (b) and 800 nm (c) excitation, respectively. These lifetimes are in very good agreement with the values obtained by Sun *et al.*

for 20 nm thin gold films ($\tau_{\text{th}}=500$ fs and $\tau_p=1$ ps.) A similar electron thermalization time of 700 fs has also been reported by Bigot *et al.*⁹ for 10 nm copper nanoparticles in a glass matrix after excitation with 620 nm femtosecond pulses.

The main difference between Figs. 2(a) and 2(b) or Fig. 2(c) is that excitation with 400 nm light (3.1 eV) leads to interband transitions from the *d*-band to the Fermi level in gold nanoparticles. The energy for the *d*-band to the Fermi surface transition in bulk gold is 2.38 eV.⁵⁰ This should also apply to the case of 20 nm particles, although an onset of this transition at 1.7 eV was reported for thiol capped nanoclusters below 2 nm in diameter.^{51,52} The excitation of interband transitions first creates excited electronic states with energies of up to 0.7 eV above the Fermi level, but also the corresponding high energetic holes in the *d*-band have to be considered. From two-photon photoemission studies on copper films it is known that the excitation of *d*-band electrons results in a 5 times faster electron–electron scattering rate.^{53–55} This, therefore, means that electron–electron scattering into the empty *d*-band states takes place on the order of the pulse duration (100 fs). Because of energy conservation for the electron–electron scattering^{47,48} a highly excited nonthermal electron distribution is formed within the conduction band, where the free electrons can have an energy of up to 3.1 eV above the Fermi level. According to Fermi liquid theory⁴⁶ this will then also cause very fast secondary electron–electron scattering events rendering a very complex behavior. Furthermore Perner *et al.* found a more efficient plasmon band damping in gold nanoparticles when interband transitions are excited.⁴ They also reported recently that the relaxation of photogenerated *d*-band holes gives a substantial contribution to the electron heating.⁶ These results confirm that interband excitations and their relaxation complicate the electron dynamics.

These complicated electron dynamics following interband excitation together with the fact, that the nonthermal electron distribution also decays by electron–phonon coupling and not only electron–electron scattering, makes the detection of an internal electron thermalization time difficult. For 630 and especially 800 nm excitation only intraband transitions are possible which lead to a smaller perturbation of the electron distribution. The same approach of selectively exciting intraband transitions in the conduction band with low power infrared femtosecond pulses was also chosen by Sun *et al.* in their studies on thin gold films.²³

It is important to point out that the excitation power was decreased until no further reduction in the measured bleach lifetimes at a still detectable signal level was observed for each excitation wavelength and it was checked by power dependence that 800 nm excitation does not lead to a two-photon absorption. The fact, that the external thermalization times for the electron–phonon coupling are nearly identical for the three excitation wavelengths, indicates that the change in electron temperature is about the same and that the results are, therefore, very well comparable with each other. The reason for the longer electron–phonon relaxation times of the 15 nm gold and 18 nm gold–silver alloy nanoparticles of 3.1 and 3.3 ps is the fact that a higher laser pump fluence

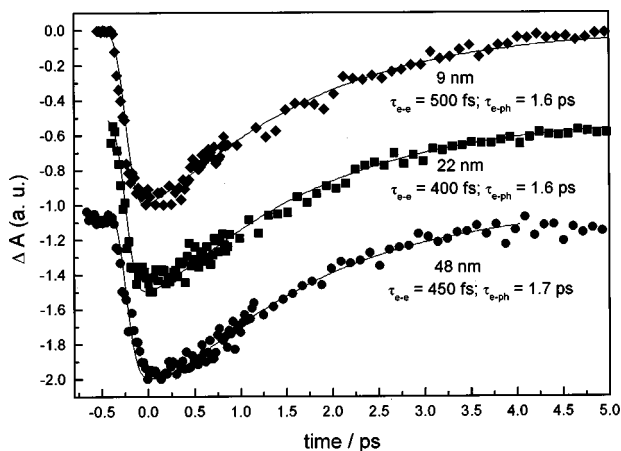


FIG. 3. Plasmon bleach recovery of 9 nm (diamonds), 22 nm (squares), and 48 nm (circles) gold particles monitored at 530 nm after excitation with 630 nm femtosecond pulses. The solid lines are fits of the experimental data to Eq. (1). Decay times of 500, 400, and 450 fs for the internal electron thermalization (electron–electron interactions τ_{e-e}) and 1.6, 1.6, and 1.7 ps for the external electron thermalization (electron–phonon interactions τ_{e-ph}) are found for the 9, 22, and 48 nm particles, respectively.

was used in order to also measure the phonon–phonon relaxation time. This will result in a higher electron temperature and because of the temperature dependence of the electronic heat capacity in an effectively longer decay time. When carrying out a series of measurements for the 15 nm gold nanoparticles with different excitation powers a limiting lifetime of about 1.7 ps on our system is also found when exciting at 400 nm and probing at 530 nm for this sample. Plotting the measured bleach decay times against the laser pump power yields a lifetime of 690 ± 100 fs and 830 ± 100 fs for zero excitation power for excitation at 400 and 630 nm, respectively. This corresponds to an electron–phonon coupling constant of $2.5 \pm 0.5 \times 10^{16} \text{ W m}^{-3} \text{ K}^{-1}$ in agreement with previous results on gold nanoparticles⁸ and bulk gold.⁹

Size dependence

The size and shape of metal nanoparticles determine the spectral position of the plasmon band absorption as well as its width. It is, therefore, interesting to study how the electron dynamics depend on the particle size. Ahmadi *et al.*³ found a size-independent electron–phonon relaxation for 1.9, 2.6, and 3.2 nm passivated gold nanocrystals and 30 nm colloidal gold. The observed spectral changes in the transient signal are attributed to changes in the density of electronic states.

While quantum size effects are dominant in these small nanocrystals, the limitation of the electron mean free path in the larger bulklike nanoparticles is an interesting question. If electron–surface scattering contributes to the relaxation of the hot electrons an increase in the measured lifetime is expected when increasing the diameter of the nanoparticles. Figure 3 shows the experimental results for 9, 22, and 48 nm gold particles. The excitation power is decreased until no further reduction in the lifetime is observed. Furthermore, the excitation power is the same for the three different sizes and their optical densities are adjusted to similar values. This leads to

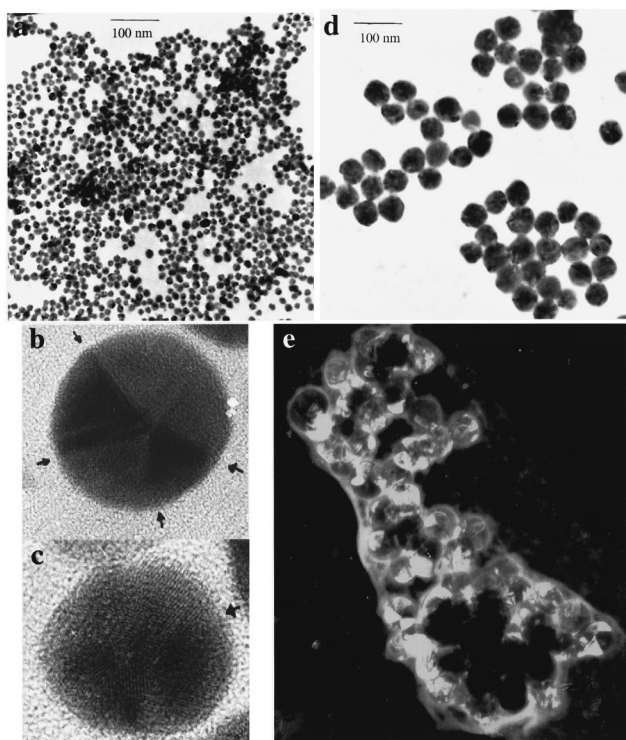


FIG. 4. Low magnification TEM image of 15 nm gold nanoparticles (a). HRTEM images of the same sample are displayed in (b) and (c). A multiple twin (b) and a stacking fault (c) can be clearly seen as indicated by the arrows. (d) and (e) show a low magnification TEM and a dark field image of 48 nm gold particles. Multiple twins and stacking faults are also present in these larger nanoparticles.

comparable changes in the electron temperature because the absorption of the nanoparticles scales with their volume according to the Mie's theory, but so does the electron heat capacity, thus canceling with each other. The excitation wavelength is 630 nm while probing at the bleach maximum. As the electron mean free path is about 50 nm in gold^{47,48} a change in the lifetimes for the three different sizes would be expected from a simple classical picture of electron-surface scattering. However the curves in Fig. 3 are fitted with decay times of 500, 400, and 450 fs for the internal electron thermalization and 1.6, 1.6, and 1.7 ps for the electron-phonon relaxation for the 9, 22, and 48 nm particles, respectively. These lifetimes are too similar to conclude a significant change in the hot electron relaxation dynamics by phonons and no contribution from electron-surface scattering effects is detectable for this size range.

Possible explanations for this behavior are: (1) Electron-surface scattering involves mainly elastic collisions and contributes only to pure dephasing processes (i.e., pure T_2), (2) the coupling to the surface phonons is less efficient because of smaller electron-phonon coupling or lower density of phonon states, or (3) as the electrons heat up via electron-electron coupling, their density on the surface atoms becomes low, leading to smaller electron-phonon coupling. Examining the same gold nanoparticles as used in the femtosecond laser studies by HRTEM, however, reveals that these metal nanoparticles contain multiple twins as well as stacking faults.⁵⁶ Figures 4(a) and 4(d) show TEM images of

15 and 48 nm gold nanoparticles. The individual lattice planes are clearly visible in the HRTEM images of the 15 nm particles [Figs. 4(b) and 4(c)]. These are typical examples of a multiply twinned particle [Fig. 4(b)] and one containing a stacking fault [Fig. 4(c)]. The average defect free volume of the 15 nm gold nanoparticles is estimated to be about only $\frac{1}{3}$ of the whole particle volume by measuring the twin boundaries in the HRTEM images and assuming tetrahedral shape. A dark-field TEM image of the 48 nm gold particles is shown in Fig. 4(e). It also shows the presence of defect structures. This is expected as the larger particles are grown by chemical reduction at room temperature from the smaller ones as nucleation centers. The core of the bigger particles, therefore, consists of the smaller nanoparticles. The HRTEM results are in agreement with studies on vacuum-evaporated gold particles (1–15 nm in diameter).^{57–59} Based on this interfacial structural information scattering of the electrons with the twin boundaries should also contribute to the electron thermalization. Even if electron-surface scattering is more effective than electron-interface scattering⁶⁰ the latter will contribute to the electron cooling and the morphology of these metal nanoparticles therefore makes the detection of a possible size effect very difficult. This could explain why no size effect is observed in this work. Furthermore, the application of a mean free path based on the particle diameter becomes at least questionable. In conclusion, a lack of a size effect on the hot electron dynamics could be related to the defect structures and the different grain sizes (very inhomogeneous distribution) present in these metal nanoparticles. In agreement with these conclusions Elsayed-Ali *et al.*^{27,29} measured an increased electron-phonon relaxation time in a polycrystalline gold film compared to a single-crystalline one. HRTEM studies on the 18 nm gold-silver alloy nanoparticles gave the same results as for the pure gold particles. The presence of defects in the alloy particles is also consistent with the similar electron-phonon relaxation times for pure gold and mixed nanoparticles (see above).

Smith *et al.*,¹³ however, found a pronounced size dependence for 15 nm gold nanoparticles compared with Au₁₃ and Au₅₅ clusters. They claim that the relaxation dynamics of the photoexcited electron gas should be described by electron-phonon coupling, which decreases with decreasing size, and electron-surface scattering, which increases with decreasing particle size. These two processes compete with each other and determine the measured lifetime. A comparison of 15 nm gold particles with small clusters consisting of just 13 and 55 atoms might however be questionable, as the description of "phonon" structure is quite different in these small size particles (or molecules).

Spectral calculations

In order to show that a non-Fermi electron distribution indeed leads to a delay in the rise of the transient absorption signal for gold nanoparticles, calculations were carried out. The response of the transient plasmon absorption in respect to a nonthermal and thermal electron distribution at a higher temperature was modeled by combining the Mie equation with a theory developed by Rosei *et al.*^{61,62} which allows one to calculate the material dielectric constant for higher elec-

tron temperatures. As the electron gas is heated by the femtosecond laser pulse, the optical constants are modified due to a different electron distribution, which leads to the observed decrease in intensity and broadening of the plasmon absorption band.

Following the model used for thin gold films²³ the differential transmission $\Delta T/T$ of the gold nanoparticles at low excitation levels can be expressed as linear combinations of the induced changes in the real and imaginary part of the dielectric constant $\Delta\epsilon_1$ and $\Delta\epsilon_2$

$$\frac{\Delta T}{T} = \frac{\delta \ln T}{\delta \epsilon_1} \cdot \Delta\epsilon_1 + \frac{\delta \ln T}{\delta \epsilon_2} \cdot \Delta\epsilon_2. \quad (2)$$

The coefficients of proportionality can be calculated using the theoretical expression for the plasmon band absorption.⁶³⁻⁶⁷ In the dipole approximation of the Mie equation the extinction cross section σ_{ext} of gold nanoparticles can be written as

$$\sigma_{\text{ext}} = \frac{9 \cdot V \cdot \epsilon_m^{(3/2)}}{c} \cdot \frac{\omega \cdot \epsilon_2(\omega)}{[\epsilon_1(\omega) + 2 \cdot \epsilon_m]^2 + \epsilon_2(\omega)^2}, \quad (3)$$

V is the spherical particle volume, c the speed of light, ω the angular frequency of the exciting radiation and ϵ_m and $\epsilon(\omega) = \epsilon_1(\omega) + i\epsilon_2(\omega)$ denote the dielectric functions of the surrounding medium (assumed to be frequency independent) and of the particle material, respectively. The data for the dielectric function of gold was taken from Ref. 68.

The changes of the real and imaginary part of the dielectric function can be related to the changes of the electron distribution function by use of the model developed by Rosei *et al.*⁶¹ for cw thermomodulation measurements. Using the constant matrix approximation, the change of the imaginary part of the dielectric function is given by²³

$$\Delta\epsilon_2 \propto \frac{1}{(h \cdot \nu)^2} \int D(E, h \cdot \nu) \cdot \Delta\rho dE, \quad (4)$$

where $D(E, h\nu)$ is the joint density of states with respect to the energy E of the final state and $\Delta\rho$ denotes the change in the electron distribution. $D(E, h\nu)$ is calculated assuming parabolic band structures for the d -band and conduction band in the vicinity of the L point of the Brillouin zone with parameters suggested by Rosei *et al.*⁶¹ This determines $\Delta\epsilon_2$ as a function of the difference in the electron distribution $\Delta\rho$. The change of the real part of the dielectric constant $\Delta\epsilon_1$ is computed using the Kramers-Kronig relationship^{47,48}

$$\Delta\epsilon_1(h \cdot \nu) = \frac{2}{\pi} \cdot P \int \frac{h \cdot \nu' \cdot \Delta\epsilon_2(h \cdot \nu')}{(h \cdot \nu')^2 - (h \cdot \nu)^2} d(h \cdot \nu'), \quad (5)$$

where P denotes a Cauchy principle value integral which extends over the whole frequency range.

The change in the electron distribution $\Delta\rho$ for a thermalized electron gas was calculated as the difference of two Fermi electron distributions $f(E, T)$ at room temperature and at a higher temperature corresponding to a certain temperature change ΔT after laser excitation. The corresponding quantity $\Delta\rho_{\text{NT}}$ for instantaneous excitation before an internal thermalization to a Fermi distribution takes place can be written as²³

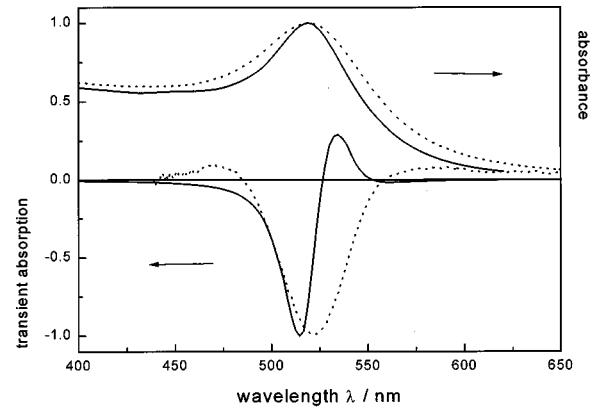


FIG. 5. Calculated (full line) and experimental (dotted line) transient absorption spectra of 22 nm gold nanoparticles. The temperature change of the electron gas is assumed to be 10 K with a thermalized Fermi distribution. Also included are the calculated (full line) and experimental (dotted line) steady-state absorption spectra.

$$\Delta\rho_{\text{NT}} = \Delta\rho_{\text{NT}}^0 \cdot \{f_0(E - E_p) \cdot [1 - f_0(E)] - f_0(E) \cdot [1 - f_0(E + E_p)]\}, \quad (6)$$

where E is the electron energy, f_0 is the Fermi distribution at the initial sample temperature T_0 (room temperature ~ 300 K), and E_p is the pump photon energy. The amplitude of the population change $\Delta\rho_{\text{NT}}$ depends on the intensity of the pump and is calculated based on the assumption that all the energy stored in the initial nonthermal distribution is redistributed among thermalized electrons. This means that the integrated change in the electron distribution is the same for the nonthermal and the thermal case.

In Fig. 5 the computed transient absorption spectrum for a temperature change of 10 K with a thermalized Fermi electron distribution is compared to a measured transient absorption spectrum. Also the calculated and measured steady-state absorption spectra of 22 nm gold nanoparticles are included. Qualitatively, the transient bleach of the plasmon band is clearly reproduced by this simple model. The minimum in the calculated spectrum at 514 nm is, however, shifted to shorter wavelength by 7 nm compared to the experimental spectrum. Also the maximum of the positive wing at lower energies is shifted in the same direction while the positive wing at higher energies could not be reproduced theoretically. These differences between the experimental and calculated spectrum might be due to the simple model assuming a parabolic band structure. The fact that the Kramers-Kronig analysis could only be carried out over the displayed energy range and not the whole frequency spectrum might also introduce an error explaining the discrepancy between the two positive absorptions at the edges of the spectrum.

Furthermore, the bandwidth of the bleach is narrower for the calculated spectrum. However, the same is true for the steady-state absorption spectrum. One reason for the different bandwidth is of course the much higher induced temperature change in the experiment which exceeds 10 K. A higher electron temperature induced by the pump laser pulse results in an increase in the transient absorption signal as well as in a broader bleach. The latter is illustrated in Fig. 6, where

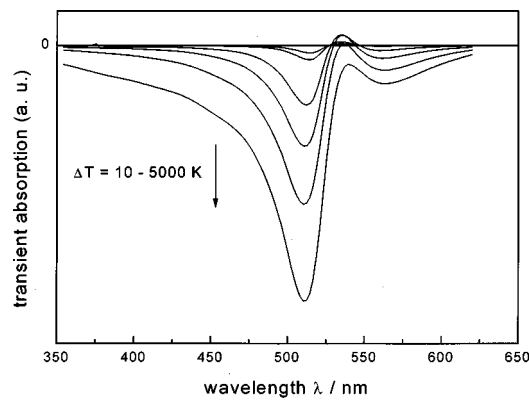


FIG. 6. Calculated transient absorption spectra for 22 nm gold nanoparticles. The temperature change ΔT of the electron gas is 10 (displayed as $\times 5$), 100, 500, 1000, 2000 and 5000 K assuming a thermalized Fermi distribution. The plasmon band bleach increases and broadens with increasing temperature change.

several transient absorption spectra calculated for electron temperature changes between 10 and 5000 K are plotted. This clearly shows that the plasmon band bleach broadens with increasing temperature corresponding to a broader plasmon band in the steady state absorption at higher electron temperatures directly reflecting a broader Fermi electron distribution.

Most important, however, is the comparison with calculations carried out assuming a nonthermal (non-Fermi) electron distribution using Eq. (6). In Fig. 7(a) the transient optical response from a non-Fermi distribution after excitation with photons of 2 eV energy resulting in a temperature change of 10 K (dashed line) is plotted together with the calculated spectrum from Fig. 6 for a Fermi electron distribution with the same temperature change (solid line). It is obvious that a nonthermal electron distribution will result in a less intense signal at the bleach maximum while at shorter wavelength it is more intense though overall small. The spectral shape is overall similar to the optical response of a thermalized electron distribution. It can, however, be concluded from these results that a non-Fermi electron distribution gives rise to a different response (less intense when monitoring at the bleach maximum) at early delay times when no internal electron thermalization has yet taken place. The signal, therefore, has a finite rise time as the maximum signal is reached after the thermalization of the excited electron gas. The reason why no slow rise in the signal but rather a flat top part of the kinetics curve is observed experimentally is that the electron gas loses its energy also by electron-phonon scattering while cooling to the Fermi distribution, as a separation of electron-electron and electron-phonon processes in time is not possible. In conclusion, it can be stated that an internal electron thermalization has to be taken into account when interpreting the experimental data. Furthermore, it is, therefore, justified to use the rate equation model [Eq. (1)]. This is in full agreement with the studies on thin gold films.^{18,19,23,24}

Finally, the effect of higher induced electron temperatures needs to be evaluated as the temperature changes by several hundred to several thousand degrees Kelvin are more

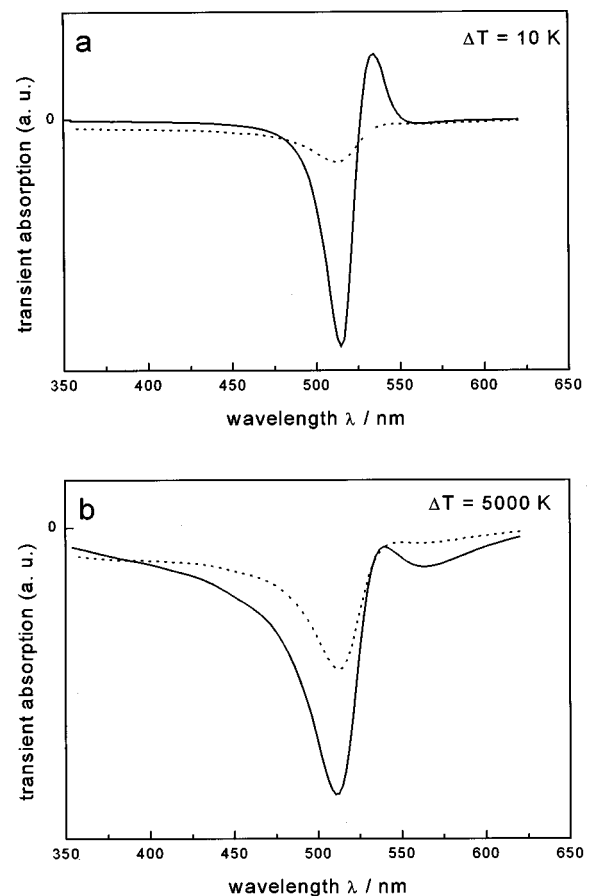


FIG. 7. Calculated transient absorption spectra for gold nanoparticles with an average diameter of 22 nm. (a) The temperature change ΔT of the electron gas is assumed to be 10 K. The solid line corresponds to the transient response of a thermalized Fermi electron distribution while the dotted line illustrates the case for a nonthermalized electron gas after excitation with photons of 2 eV energy. (b) The temperature change ΔT of the electron gas is assumed to be 5000 K. The solid line corresponds to the transient response of a thermalized Fermi electron distribution while the dotted line illustrates the case for a nonthermalized electron gas after excitation with photons of 2 eV energy. Comparison of the two pictures leads to the conclusion that the relative difference of a nonthermalized and thermalized electron distribution decreases with increasing temperature change ΔT (excitation power). The detection of a nonthermal electron distribution is, therefore, complicated at high pump fluences.

realistic. Figure 7(b) shows the calculated spectra for a nonthermal and a thermal electron distribution with a change in the electron temperature by 5000 K. Only relative intensities are plotted for the calculated spectra. However, comparing the results for the temperature change of 10 K with the one for 5000 K in Figs. 7(a) and 7(b), it becomes obvious that the relative difference between the signal of the thermalized to the nonthermalized electron distribution decreases with an increasing temperature change. This difference, therefore, decreases with increasing laser power of the pump pulse. Because of the similar spectral response from the thermalized compared to the nonthermalized electron distribution a deviation in the time evolution of the experimental signal from a single exponential behavior is only expected for a large difference in the intensities of the two electron distributions. This leads then to the conclusion that the effect of a nonthermal electron distribution on the differential transmis-

sion spectrum of gold nanoparticles will be more pronounced at low excitation power (low perturbation limit) and might not be detectable at all at high laser fluences.

CONCLUSION

15 nm gold and 18 nm gold-silver alloy nanoparticles show very similar electron dynamics when probed under the same excitation conditions. Electron-phonon and phonon-phonon relaxation times of 3.1 and 90 ps for the gold nanoparticles and 3.3 and 86 ps for the alloy nanoparticles are measured after exciting at 400 nm. The plasmon band bleach for the alloy nanoparticles is found around 500 nm in agreement with a blueshifted plasmon absorption in the steady-state spectrum. Thus dissolving silver in gold nanoparticles shifts the plasmon frequency, but has no effect on the electron cooling dynamics. This means that the gold-silver system is suitable to form very homogeneous alloy nanoparticles with tunable optical properties as the plasmon absorption and therefore the transient bleach can be tuned continuously between 400 and 520 nm depending on the gold mole fraction without changing its nonradiative response. At low excitation power we find strong evidence for a non-Fermi electron distribution which thermalizes to an equilibrium distribution corresponding to a higher electron temperature with a lifetime of 500 fs. The temporal behavior of the bleach of the plasmon band can be modeled with the assumption of an initially non-Fermi electron distribution which decays by electron-electron scattering while at the same time electron-phonon interactions take place and dominate the kinetics once a thermalized electron distribution is reached. The last process has been evaluated with a relaxation time of 1.7 ps. A finite electron thermalization with a decay time of 500 fs can be used in the fit only if low excitation powers are used to excite mainly the intraband transitions, thus leading to a small perturbation of the electron gas. The results presented here are in excellent agreement with studies on 20 nm thin gold films.^{23,24} Furthermore, simulations of the optical response arising from a thermalized and a nonthermalized electron distribution can confirm these conclusions. While the absence of a size dependence in our transient absorption studies of 9, 22, and 48 nm gold nanoparticles could be a result of the cancellation of two competing size-dependent factors such as the electron-phonon coupling and the density of states, we suggest that electron scattering with twin boundaries or other interfaces arising from defect structures within the nanoparticles could be the dominant scattering process resulting in the observed size independence.

ACKNOWLEDGMENTS

This work was supported by NSF (Grant No. CHE 9705164). S.L. wishes to thank the German Fond der Chemischen Industrie and the German BMBF for a Ph.D. fellowship. C.B. likes to thank the Swiss National Science Foundation.

¹A. P. Alivisatos, *J. Phys. Chem.* **100**, 13226 (1996).

²T. S. Ahmadi, S. L. Logunov, and M. A. El-Sayed, *J. Phys. Chem.* **100**, 8053 (1996).

- ³T. S. Ahmadi, S. L. Logunov, M. A. El-Sayed, J. T. Khoury, and R. L. Whetten, *J. Phys. Chem. B* **101**, 3713 (1997).
- ⁴M. Perner, P. Bost, G. V. Plessen, J. Feldmann, U. Becker, M. Mennig, and H. Schmidt, *Phys. Rev. Lett.* **78**, 2192 (1997).
- ⁵M. Perner, P. Bost, T. Pauck, G. v. Plessen, J. Feldmann, U. Becker, M. Mennig, J. Porstendorfer, M. Schmitt, and H. Schmidt, in *Ultrafast Phenomena X*, edited by P. F. Babara, J. G. Fujimoto, W. H. Knox, and W. Zinth (Springer, Berlin, 1996).
- ⁶M. Perner, T. Klar, S. Grosse, U. Lemmer, G. v. Plessen, W. Spirkl, and J. Feldmann, *J. Lumin.* **76&77**, 181 (1997).
- ⁷J. K. Hodak, I. Martini, and G. V. Hartland, *J. Phys. Chem. B* **102**, 6958 (1998).
- ⁸J. K. Hodak, I. Martini, and G. V. Hartland, *Chem. Phys. Lett.* **284**, 135 (1998).
- ⁹J.-Y. Bigot, J.-C. Merle, O. Cregut, and A. Daunois, *Phys. Rev. Lett.* **75**, 4702 (1995).
- ¹⁰T. W. Roberti, B. A. Smith, and J. Z. Zhang, *J. Chem. Phys.* **102**, 3860 (1995).
- ¹¹B. A. Smith, D. M. Waters, A. E. Faulhaber, M. A. Kreger, T. W. Roberti, and J. Z. Zhang, *J. Sol-Gel Sci. Technol.* **9**, 125 (1997).
- ¹²A. E. Faulhaber, B. A. Smith, J. K. Andersen, and J. Z. Zhang, *Mol. Cryst. Liq. Cryst.* **283**, 25 (1996).
- ¹³B. A. Smith, J. Z. Zhang, U. Giebel, and G. Schmid, *Chem. Phys. Lett.* **270**, 139 (1997).
- ¹⁴H. Inouye, K. Tanaka, I. Tanahashi, and K. Hirao, *Phys. Rev. B* **57**, 11334 (1998).
- ¹⁵T. Tokizaki, A. Nakamura, S. Kaneko, K. Uchida, S. Omi, H. Tanji, and Y. Asahara, *Appl. Phys. Lett.* **65**, 941 (1994).
- ¹⁶G. Schmid, *Clusters & Colloids: From Theory to Application* (VCH, Weinheim, 1994).
- ¹⁷A. S. Edelstein and R. C. Cammarata, *Nanoparticles: Synthesis, Properties and Applications* (Institute of Physics Publishing, Bristol, 1996).
- ¹⁸M. J. Feldstein, C. D. Keating, Y.-H. Liau, M. J. Natan, and N. F. Scherer, *J. Am. Chem. Soc.* **119**, 6638 (1997).
- ¹⁹R. H. M. Groeneveld, R. Sprik, and A. Lagendijk, *Phys. Rev. B* **51**, 11433 (1995).
- ²⁰R. H. M. Groeneveld, R. Sprik, and A. Lagendijk, *Phys. Rev. B* **45**, 5079 (1992).
- ²¹G. L. Esley, *Phys. Rev. B* **33**, 2144 (1986).
- ²²G. L. Esley, *Phys. Rev. Lett.* **51**, 2140 (1983).
- ²³C.-K. Sun, F. Vallee, L. H. Acioli, E. P. Ippen, and J. G. Fujimoto, *Phys. Rev. B* **50**, 15337 (1994).
- ²⁴C.-K. Sun, F. Vallee, L. H. Acioli, E. P. Ippen, and J. G. Fujimoto, *Phys. Rev. B* **48**, 12365 (1993).
- ²⁵R. W. Schoenlein, W. Z. Lin, J. G. Fujimoto, and G. L. Esley, *Phys. Rev. Lett.* **58**, 1680 (1987).
- ²⁶S. D. Brorson, J. G. Fujimoto, and E. P. Ippen, *Phys. Rev. Lett.* **59**, 1962 (1987).
- ²⁷T. Juhasz, H. E. Elsayed-Ali, G. O. Smith, C. Suarez, and W. E. Bron, *Phys. Rev. B* **48**, 15488 (1993).
- ²⁸T. Juhasz, H. E. Elsayed-Ali, H. Hu, and W. E. Bron, *Phys. Rev. B* **45**, 13819 (1992).
- ²⁹H. E. Elsayed-Ali, T. Juhasz, G. O. Smith, and W. E. Bron, *Phys. Rev. B* **43**, 4488 (1991).
- ³⁰C. A. Schmuttenmaer, M. Aeschlimann, H. E. Elsayed-Ali, R. J. D. Miller, D. A. Mantell, J. Cao, and Y. Gao, *Phys. Rev. B* **50**, 8957 (1994).
- ³¹M. Aeschlimann, C. A. Schmuttenmaer, H. E. Elsayed-Ali, R. J. D. Miller, J. Cao, Y. Gao, and D. A. Mantell, *J. Chem. Phys.* **102**, 8606 (1995).
- ³²Y. Gao, J. Cao, R. J. D. Miller, H. E. Elsayed-Ali, and D. A. Mantell, *Phys. Rev. B* **56**, 1099 (1997).
- ³³E. Knoesel, A. Hotzel, T. Hertel, M. Wolf, and G. Ertl, *Surf. Sci.* **368**, 76 (1996).
- ³⁴W. S. Fann, R. Storz, H. W. K. Tom, and J. Boker, *Phys. Rev. B* **46**, 13592 (1992).
- ³⁵W. S. Fann, R. Storz, H. W. K. Tom, and J. Boker, *Phys. Rev. Lett.* **68**, 2834 (1992).
- ³⁶P. B. J. Allen, *Phys. Rev. Lett.* **59**, 1460 (1987).
- ³⁷D.-S. Kim, J. Shah, J. E. Cunningham, T. C. Damen, S. Schmitt-Rink, and W. Scafer, *Phys. Rev. Lett.* **68**, 2838 (1992).
- ³⁸O. B. Wright, *Phys. Rev. B* **49**, 9985 (1994).
- ³⁹S. Link and M. A. El-Sayed, *J. Phys. Chem. B* (in press).

- ⁴⁰J. Turkevich, P. C. Stevenson, and J. Hillier, *Discuss. Faraday Soc.* **11**, 55 (1951). This method yields spherical particles with an average diameter of about 20 nm. While the actual value of the mean size might vary slightly from each preparation the size distribution was, however, found to be always about 10%.
- ⁴¹D. A. Handley, *Colloidal Gold: Principles, Methods, and Applications* (Academic, New York, 1989), Vol. 1.
- ⁴²J. Turkevich, G. Garton, and P. C. Stevenson, *J. Colloid Sci. Supplement* **1**, 26 (1954).
- ⁴³J. Turkevich, *Gold. Bull.* **18**, 86 (1985).
- ⁴⁴S. Link, Z. L. Wang, and M. A. El-Sayed, *J. Phys. Chem. B* **103**, 3529 (1999).
- ⁴⁵E. J. Heilweil and R. M. Hochstrasser, *J. Chem. Phys.* **82**, 4762 (1985).
- ⁴⁶D. Pines and P. Nozieres, *The Theory of Quantum Liquids* (Benjamin, New York, 1966).
- ⁴⁷N. W. Ashcroft and N. D. Mermin, *Solid State Physics* (Saunders College, Philadelphia, 1976).
- ⁴⁸C. Kittel, *Introduction to Solid State Physics* (Wiley, New York, 1996).
- ⁴⁹L. Anisimov, B. L. Kapeliovich, and T. L. Perel'man, *Sov. Phys. JETP* **39**, 375 (1975).
- ⁵⁰N. E. Christensen and B. O. Seraphin, *Phys. Rev. B* **4**, 3321 (1971).
- ⁵¹T. G. Schaaff, M. N. Shafigullin, J. T. Khoury, I. Vezmar, R. L. Whetten, W. G. Cullen, P. N. First, C. Gutierrez-Wing, J. Ascencio, and M. J. Jose-Yacanan, *J. Phys. Chem. B* **101**, 7885 (1997).
- ⁵²M. M. Alvarez, J. T. Khoury, T. G. Schaaff, M. N. Shafigullin, I. Vezmar, and R. L. Whetten, *J. Phys. Chem. B* **101**, 3706 (1997).
- ⁵³S. Pawlik, M. Bauer, and M. Aeschlimann, *Surf. Sci.* **377–379**, 206 (1997).
- ⁵⁴M. Aeschlimann, S. Pawlik, and M. Bauer, *Ber. Bunsenges. Phys. Chem.* **99**, 1504 (1995).
- ⁵⁵S. Ogawa and H. Petek, *Surf. Sci.* **357–358**, 585 (1996).
- ⁵⁶Z. L. Wang, *Adv. Mater.* **10**, 13 (1998).
- ⁵⁷P.-A. Buffat, M. Flueeli, R. Spycher, P. Stadelmann, and J.-P. Borel, *Faraday Discuss.* **92**, 173 (1991).
- ⁵⁸D. J. Smith and L. D. Marks, *J. Cryst. Growth* **54**, 433 (1981).
- ⁵⁹D. J. Smith and L. D. Marks, *J. Cryst. Growth* **54**, 425 (1981).
- ⁶⁰Z. L. Wang, *Elastic and Inelastic Scattering in Electron Diffraction and Imaging* (Plenum, New York, 1995).
- ⁶¹R. Rosei, F. Antongeli, and U. M. Grassano, *Surf. Sci.* **37**, 689 (1973).
- ⁶²M. Cardona, in *Modulation Spectroscopy, Solid State Physics Supplement II*, edited by F. Seitz, D. Turnbull, and H. Ehrenreich (Academic, New York, 1969).
- ⁶³G. Mie, *Ann. Phys. (Leipzig)* **25**, 377 (1908).
- ⁶⁴U. Kreibitz and M. Vollmer, *Optical Properties of Metal Clusters* (Springer, Berlin, 1995).
- ⁶⁵G. C. Papavassiliou, *Prog. Solid State Chem.* **12**, 185 (1980).
- ⁶⁶M. Kerker, *The Scattering of Light and Other Electromagnetic Radiation* (Academic, New York, 1969).
- ⁶⁷C. F. Bohren and D. R. Huffman, *Absorption and Scattering of Light by Small Particles* (Wiley, New York, 1983).
- ⁶⁸P. B. Johnson and R. W. Christy, *Phys. Rev. B* **6**, 4370 (1972).